

ON THE SHARP BEND IN THE S-N CURVE OF THE AZ31 EXTRUDED MAGNESIUM ALLOY

Zhenyu NAN, Sotomi ISHIHARA^{*}, Takahito GOSHIMA, and Reiko NAKANISHI

^{*}Department of Mechanical and Intellectual System Engineering, Toyama University
3190 Gofuku, Toyama-shi, Toyama, 930-8555 Japan
ishi@eng.toyama-u.ac.jp

Abstract

Rotating bending fatigue test was carried out using AZ31 extruded magnesium alloy in order to clarify the S-N curve, crack initiation and propagation behaviour of the alloy. The present material is divided roughly into 2 kinds of banded texture, the phase A and B. The phase B further consists of the crystal grains (phase C). The fatigue crack generates at the upper and lower edges of the grain boundary (phase C) in the early stage of the fatigue life. At stress amplitude of 122.5 MPa which is slightly larger than the fatigue limit, the crack develops to the next B-phase without being blocked by the grain boundary (phase B), however at 120 MPa which is slightly less than the fatigue limit, the crack advance was blocked by the grain boundary. The sharp curved S-N curve is attributable to the crack arrest, which is caused by the grain boundary of the phase B.

Key Words: Fatigue, Magnesium alloy, S-N curve, Fatigue crack, Crack initiation, Crack propagation, Crack arrest.

1. Introduction

Magnesium alloys are very attractive as structural materials, because they are extremely light, possessing excellent specific tensile strength, good stiffness and vibrational absorption [1]. However, magnesium alloys have not been used extensively until recently because of their vulnerability to corrosion and their high cost. Now, due to their energy and weight saving characteristics, magnesium alloys are considered to be good candidates as materials in, for example, auto parts, portable personal computers and telephones. When considering the use of magnesium alloys as structural materials, a thorough understanding of the fatigue characteristics is necessary.

Goodenberger *et al.* [2] studied the fatigue behavior of cast magnesium alloy, AZ91E-T6 in laboratory air. Kobayashi *et al.* [3] investigated the influence of the corrosive environment on the fatigue characteristics of the AZ31 magnesium alloy. Hilpert *et al.* [4] also studied the corrosion fatigue behavior of the AZ80 magnesium alloys that are received various surface treatments, such as electro-polishing, grinding, machining and shot-peened. They clarified that corrosion fatigue lives become shorter in comparison with those in a laboratory air. Eisenmeier *et al.* [5] studied the fatigue behavior of AZ91 magnesium alloy, which was processed by the vacuum die casting method. They reported that the fatigue cracks generate from the casting defects involved in the material, and the crack growth behavior is influenced by the microstructure of the material. Shih *et al.* [6] performed the rotating bending fatigue experiment on the extruded magnesium alloy AZ61A. They reported that cracks generate from the inclusions, which exist on the specimen surface or the vicinity of the surface, and

the initial crack growth behavior is affected by the specimen microstructure. Kobayashi *et al.* [7] studied the fatigue crack growth characteristic of the AZ91D and AM60B magnesium alloy. They clarified that the atmosphere causes hydrogen brittleness of the material, and brings acceleration in the fatigue crack growth by this brittleness. Sajuri *et al.* [8] studied the effect of the humidity on the fatigue characteristics of the AZ61 alloy. They reported that in the high humidity, corrosion pit arises in the early stage of fatigue process of the specimen, and its failure is easily caused because of the crack generation from these corrosion pits.

As reviewed above, many researches addressing the effect of environment on fatigue characteristics of the magnesium alloys have been done so far, however the researches on fatigue mechanism are very few. Therefore, it cannot necessarily be said that the fatigue failure mechanisms for the magnesium alloys have been clarified.

In the present study, to accumulate the basic data about the fatigue characteristic of a magnesium alloy, the fatigue experiments were conducted using an extruded magnesium alloy AZ31. The S-N characteristic and the fatigue crack initiation and growth behavior during the fatigue process of the material were studied in detail, while observing the influence of the material microstructure.

2. Material and experimental method

2.1 Material

The magnesium alloy AZ31 used in the present experiment was obtained by extruding a billet with a diameter of 88.9 mm into a round bar 19 mm in diameter. Its chemical composition and mechanical properties are listed in Tables 1 and 2, respectively.

TABLE 1. Chemical compositions of the material. (wt%)

| Al | Zn | Mn | Fe | Ni | Cu | Si | Ca | Mg |
|------|------|-------|-------|-------|-------|------|------|------|
| 2.98 | 0.97 | 0.004 | 0.007 | 0.005 | 0.002 | 0.02 | 0.05 | Bal. |

TABLE 2. Mechanical property of the material.

| Yield Strength | Tensile Strength | Elongation | Young's modulus |
|----------------|------------------|------------|-----------------|
| 200 MPa | 275 MPa | 11 % | 45 GPa |

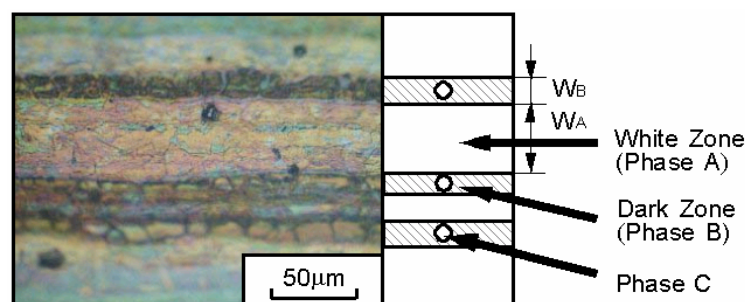


FIGURE 1. Microstructure of the AZ31 alloy.

TABLE 3. Composition and Vickers hardness of the microstructure.

| Structure | Composition | Vickers hardness | Typical size(μm) |
|-----------|--|------------------|-------------------------------|
| A | Mg | 61 | $W_A=40$ |
| B | $\text{Mg}_{32}(\text{Al},\text{Zn})_{49}$ | 93 | $W_B=24$ |
| C | $\text{Mg}_{17}\text{Al}_{12}$ | 83 | $d_i=20$ |

Fig. 1 shows a photograph of the material microstructure for the plane, which is parallel to the extrusion direction. A schematic illustration is appended to the figure on the right side of the figure for descriptions. As seen from the photograph, the microstructure consists of two types of lamellar structures, the white part (phase A) and the black part (phase B). Both lamellar structures are layered alternately and parallel to the extrusion direction. In addition, a separate crystal structure (phase C) can be observed inside the B phase. Analysis of the composition of each phase was done using Electron Probe Micro Analyzer (EPMA, Shimadzu, EPMA-1500) and X-ray diffraction equipment (Rigaku, RINT2200/PC/K). The EPMA plane analysis revealed that the white part (phase A) is pure magnesium, the black part (phase B) is the intermetallic compound (Mg-Al-Zn system), and the C phase is the intermetallic compound (Mg-Al system). Identification using X-ray diffraction showed that phases B and C were $\text{Mg}_{32}(\text{Al}, \text{Zn})_{49}$ and $\text{Mg}_{17}\text{Al}_{12}$, respectively. The representative dimensions of the material microstructure, such as the widths of phases A and B and the grain diameter of phase C were measured using an optical microscope.

Table 3 shows the results of the X-ray diffraction, the representative dimensions and the micro hardnesses for phases A, B, and C. The micro hardness of each phase was measured using a micro hardness tester (Akashi, HM-102). W_A and W_B in the table show the width of phases A and B, respectively, whereas d_i is the grain size of phase C. According to this table, the hardness of phases B and C are $H_V=93$ and $H_V=83$, respectively. These hardnesses are clearly greater than that of phase A, $H_V=61$. We can also see that the average sizes of the microstructures (W_A , W_B , d_i) are 40, 24, 20 μm , respectively.

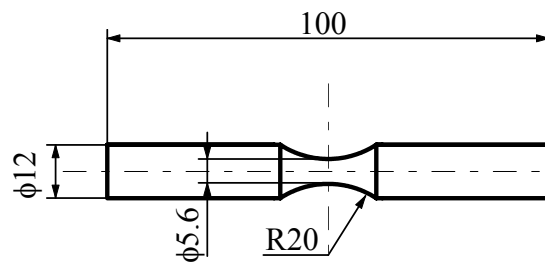


FIGURE 2. Shape and dimensions of the specimen (mm).

2.2 Experimental method

Fatigue tests were performed using specimens with a configuration (stress concentration factor =1.04) as shown in Fig. 2. The specimen was machined from a round bar 19 mm in diameter. The specimen was prepared for the experiment by polishing its surface to a mirror-like finish with emery paper and diamond paste.

Fatigue tests were performed using a cantilever-type rotating bending fatigue machine in a laboratory air with humidity of 63~73 % at temperature of 298 K. In addition, special control

of temperature or humidity was not done during the experiment. The stress cyclic speed was 30 Hz.

The replicas of the specimen surfaces were collected during the fatigue process by interrupting the test at a fixed number of cycles to investigate the initiation and growth behaviour of fatigue cracks. Crack lengths were measured by observing the replicas using an optical microscope (OLIMPUS, STM) and digital camera (OLYMPUS, DP10) at magnification of 400. In addition, in order to investigate the effect of the material microstructure on the crack initiation and growth behaviour, some specimens were tested with revealing their surface organizations by using etching liquid. Fracture surfaces of the specimens were observed using a scanning electron microscope (Hitachi, S-530).

3. Experimental results

3.1 S-N curve

Fig. 3 shows S-N curve of Magnesium alloy AZ31 at a stress ratio $R=-1$ and stress cyclic speed of $f=30$ Hz in a laboratory air. As seen from the figure, the fatigue life at stress amplitude of 120 MPa is 5.14×10^7 cycle while it is only 8.5×10^4 cycle at 122.5 MPa, which is larger than the former by only 2.5 MPa. The difference in the stress amplitude of only 2.5 MPa makes the fatigue life difference as many as 600 times difference. As a result, a sharp bend is observed in the S-N curve. The solid line in the figure will be explained later.

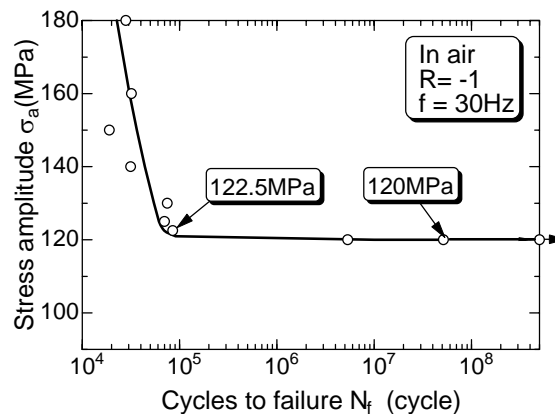


FIGURE 3. S-N curve for the AZ31 alloy in laboratory air.

3.2 Successive Observation of Fatigue Process

In order to clarify the reason why the slight difference in the stress amplitude has a big influence on a fatigue life, the successive observations of the specimen surface during the fatigue process at stress amplitude of 120 MPa and 122.5 MPa were performed using the replica method.

Fig. 4 shows the successive observation result of the specimen surface during the fatigue process at stress amplitude of 120 MPa. As seen from the figure, the crack is initiated in the crystal grain of the phase C at 7.34×10^6 cycles (Fig. 4 (B)). Then, the crack propagates to the size of $22.5 \mu\text{m}$ equivalent to the grain diameter of the phase C by the stress repetition of 2.45×10^7 cycles (Fig. 4 (C)). After that, the crack propagation is prevented by the grain boundary over the long time.

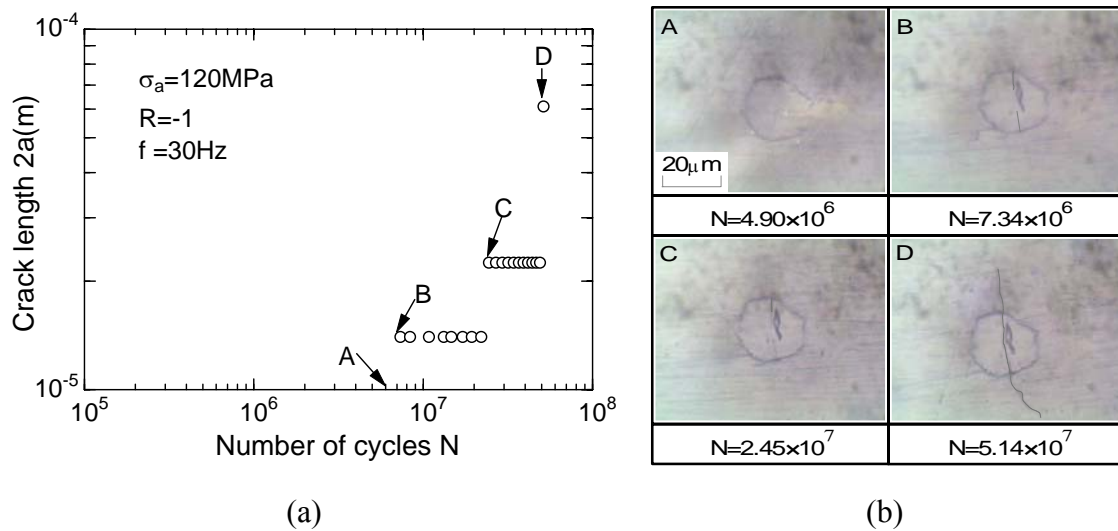


FIGURE 4. Successive observations of the specimen surface during the fatigue process ($\sigma_a = 120$ MPa).

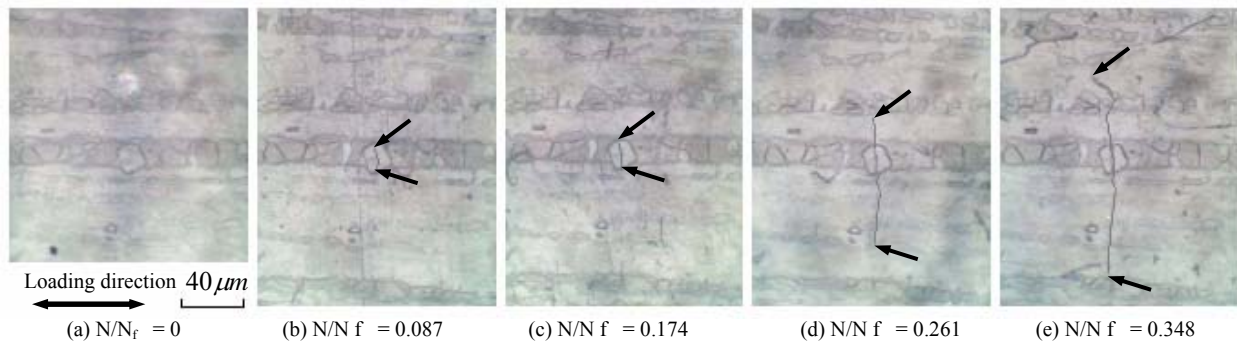


FIGURE 5. Successive observations on a specimen surface during the fatigue process ($\sigma_a = 122.5$ MPa).

By the stress repetition over the long period of 5.14×10^7 cycles (Fig. 4 (D)), the crack at last ran through the grain boundary, and grew to length of $61 \mu\text{m}$, then followed by the final failure of the specimen.

Fig. 5 shows the successive observation results of the specimen surface during the fatigue process of stress amplitude of 122.5 MPa. In order to investigate the effect of the specimen microstructure on the crack initiation and growth behaviour, the successive observations were conducted after revealing the specimen microstructure by etching. In the figures, the arrow is attached to specify the crack tip. As seen from the figure, a crack initiates by the stress repetition at the phase C (Fig. 5 (b)), which is the black portion in the figure (Dark zone). Afterwards the crack (Fig.5 (c)) propagated to the neighbour phase (Fig.5 (d)).

Such characteristic at the stress amplitude of 122.5 MPa in Fig. 5 is common to the result in the stress amplitude of 120 MPa in Fig. 4 except for that the crack stationary period at the grain boundary in the former is shorter than in the latter. It was also observed that the rate of crack growth lowers when the crack cross the black lamellar structure (Dark Zone), and that the propagation direction bends to aslant (Fig. 5 (e)). Though the figure was omitted, such crack growth features were also observed in the observations at stress amplitude of 140 MPa.

3.3 Characteristic of fatigue crack growth

Fig. 6 shows the variations of crack length as a function of fatigue life ratio N/N_f that was measured from the successive observation during the fatigue process. In the figure, the data for three different stress amplitudes are plotted. We can see no stress amplitude dependency in the relation $2a$ vs. N/N_f . As seen from this figure, in the fatigue process for the stress amplitudes of 122.5 and 140 MPa, a crack with size of 20 μm in length initiates at the very early stage of fatigue life, 5~6 % of the fatigue life ratio. Therefore, the total fatigue life is thought to be the crack growth life.

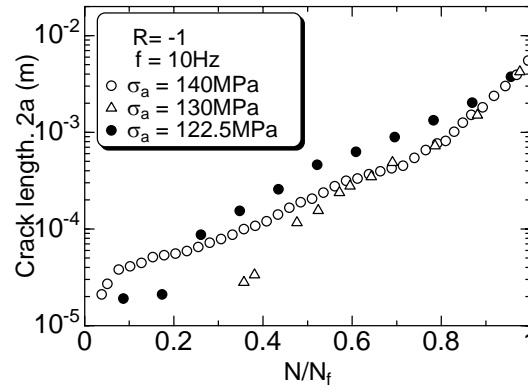


FIGURE 6. Variations of crack lengths as a function of fatigue life ratio N/N_f .

When applying the linear elastic fracture mechanics (LEFM) to the small crack, it is always pointed out that the application of the LEFM should be restricted, since the ratio of the plastic zone size at the crack tip to the crack length is large, and resulting the deviation from the small scale yielding condition in the small crack [9].

However, the application of linear elastic fracture mechanics is useful from the practical viewpoint. So in the following, we try to analyze the crack growth behaviour of the present material by using LEFM. Fig. 7 shows the relationship between crack growth rate da/dN and stress intensity factor range ΔK . For a calculation of ΔK , the following equation was used.

$$\Delta K = 1.04Y\sigma_a\sqrt{\pi a} \quad (1)$$

where, 1.04 indicates a stress concentration factor due to the specimen's notch with radius R20, and Y is a correction factor for the surface crack with a semi-circular shape ($=0.73$) and a denotes a half crack length. As seen from the figure, a clear stress amplitude dependence is not seen in the relation da/dN vs. within the stress amplitude range of 120~160 MPa. A ratio of a plastic zone size at a crack-tip to the total crack length is 10 % or less even at the maximum stress of 160 MPa, and at the low stress amplitude range, the ratios take quite low values of 4~5 %. Therefore, this may be the reason why the large elasto-plastic effect did not appear in the da/dN - ΔK relation. In Fig. 7, the relation da/dN - ΔK for a long through crack, which was investigated by D. L. Goodenberger using on AZ91E-T6 cast-alloy [2], is shown by the broken line. As seen from the figure, the da/dN vs. ΔK relations for the small surface crack and for the long through crack almost agree with each other, except for that the crack growth threshold for the small surface crack ($0.44 \text{ MPa}\sqrt{\text{m}}$) is lower than that for the long through crack ($0.9 \text{ MPa}\sqrt{\text{m}}$), and that the rate of crack growth for the former is faster than the latter in the lower ΔK region. From Fig.7, the following expression can be obtained for the crack growth law.

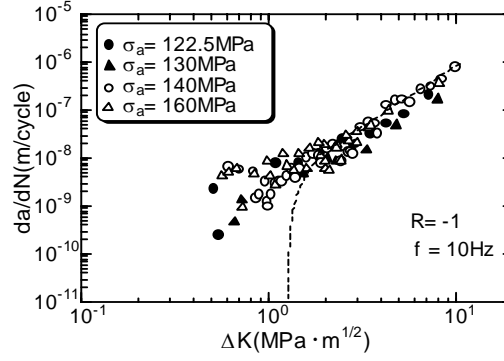


FIGURE 7. Fatigue crack growth rate as a function of ΔK .

$$da/dN = A(1.04Y\sigma_a\sqrt{\pi a} - \Delta K_{th})^2 \quad (2)$$

where, A ($= 7 \times 10^{-9} MPa^{-2}$) and ΔK ($= 0.44 MPa\sqrt{m}$) are material constants.

4. Discussions

4.1 Sharp bend in the S-N curve

The fatigue crack generates at the upper and lower edges of the grain boundary (C phase) in the early stage of the fatigue life, and soon coalesces with each other. Then the crack tries to develop further from the phase C to the phase B. However, it is difficult for the crack to grow further when the applied stress is low because the phase B is harder than the phase C as shown in Table 3. In the S-N curve of Fig. 3, a crack is blocked for a long time by the hard phase B at the low stress amplitude of 120 MPa. However at the slightly larger stress amplitude of 122.5 MPa, a crack easily grew without being blocked at boundary of hard phase B. It seems that only 2.5 MPa difference in the stress amplitude determines whether a crack can propagate into the phase B or not. Therefore, the reason why the sharp bend was observed in the S-N curve of the present magnesium alloy is that the crack was blocked at the boundary between phase C and B when the crack develops from the phase C to the phase B. Such thought coincides well with the experimental observation that a crack is easy to stagnate with an increase in the thickness of the phase B, which surrounds the phase C where the crack initiates.

Until now, it is reported [9] that a stationary crack exists at fatigue limit of carbon steel due to a work hardening and strain aging at the crack tip by the stress cycling. However in the present study, the specimen hardness during fatigue process hardly changed. So the work hardening and strain aging may have little relationship with the crack arrest and sharp bend of the S-N curve observed in the present study.

4.2 Estimation of fatigue lives from the crack growth law.

By integrating Eq. (2) from an initial half crack length ($a_i=10 \mu m$) to the one ($a_f=3 mm$) at the specimen failure, crack propagation life N_p can be obtained by the following expression.

$$N_p = \frac{2}{AB^2} \ln \frac{B\sqrt{a_f} - \Delta K_{th}}{B\sqrt{a_i} - \Delta K_{th}} - \frac{2}{AB^2} \left(\frac{\Delta K_{th}}{B\sqrt{a_f} - \Delta K_{th}} - \frac{\Delta K_{th}}{B\sqrt{a_i} - \Delta K_{th}} \right) \quad (3)$$

where, B is given as $B = 1.04Y\sigma\sqrt{\pi}$.

As stated before, a crack initiation life can be neglected as compared with a crack propagation life. So, we can consider that Eq. (4) represent a whole fatigue life. The solid curve in Fig. 3 shows estimations of fatigue lives from Eq. (4). From the figure, the estimation corresponds well to the experimental results including near the fatigue limit. This result indicates that the total of fatigue life can be almost considered as the crack propagation life.

5. Conclusions

Completely reversed bending fatigue tests were performed on extruded magnesium alloy AZ31 using smooth specimens to study crack initiation and propagation behaviour for the material. The results obtained can be summarized as follows.

- (1) A sharp bend was observed in the S-N curve of the present extruded magnesium alloy.
- (2) Fatigue cracks initiated at the grain boundary between phase B and C at an early stage of fatigue life. Afterwards the crack propagated through the phase C and tried to propagate the next phase B. At fatigue limit of 120 MPa, the crack was blocked for a long time by the phase B, however at 122.5 MPa which is slightly higher than the fatigue limit, a crack propagated easily into the phase B without being blocked.
- (3) The sharp bend in S-N curve is attributable to the crack arrest by the phase B.
- (4) S-N curve was estimated by integrating the crack growth law. The estimated result agrees well with an experimental result.

References

1. Kojima Y., *Handbook Advanced Magnesium Technology*, Kallos Publishing Co., Ltd., Tokyo, Japan, 2000.
2. Goodenberger D.L., Stephens R.I., *Journal of Engineering Materials and Technology*, vol. **115**, 391-397, 1993.
3. Kobayashi Y., Takano K., Ishikawa K., Program of The 96th Conference of Japan Institute of Light Metals, 1999, 81-82.
4. Hilpert M., Wagner L., *Journal of Materials Engineering and Performance*, vol. **9** (4), 402-407, 2000.
5. Eisenmeier G., Holzwarth B., Hoppel H.W., Mughrabi H., *Materials Science Engineering A*, vol. **319**, 578-582, 2001.
6. Shih T.S., Liu W.S., Chen Y.J., *Materials Science Engineering A*, vol. **325**, 152-162, 2002.
7. Kobayashi Y., Takano K., Ishikawa K., Program of The 94th Conference of Japan Institute of Light Metals, 1998, 267-268.
8. Sajuri Z.B., Umehara T., Miyashita Y., Mutoh Y., *Fatigue 2002: Proceedings of the Eighth International Fatigue Conferences*. Blom AF, editor. EMAS, West Midlands, UK, 2002, 3301-3308.
9. Nishitani H., *Fatigue strength*, Ohmsha. Ltd.; Tokyo, Japan, 1985.